arXiv:1407.0914v3 [astro-ph.GA] 6 Sep 2014

v2.3 Tuesday 9th September, 2014 01:18

A TALE OF THREE GALAXIES: ANOMALOUS DUST PROPERTIES IN IRAS F10398+1455, IRAS F21013-0739 AND SDSS J0808+3948

Yanxia Xie[1,2], Lei Hao[1†], and Aigen Li[2]

ABSTRACT

On a galactic scale the 9.7 μm silicate *emission* is usually only seen in type 1 active galactic nuclei (AGNs). They usually also display a *flat* emission continuum at $\sim$5–8 μm and the absence of polycyclic aromatic hydrocarbon (PAH) emission bands. In contrast, starburst galaxies, luminous infrared (IR) galaxies (LIRGs), and ultraluminous IR galaxies (ULIRGs) exhibit a *red* 5–8 μm emission continuum, strong 9.7 μm and 18 μm silicate *absorption* features, and strong PAH emission bands. Here we report the detection of anomalous dust properties by *Spitzer*/Infrared Spectrograph in three galaxies (IRAS F10398+1455, IRAS F21013-0739 and SDSS J0808+3948) which are characterized by the simultaneous detection of a *red* 5–8 μm emission continuum, the 9.7 and 18 μm silicate *emission* features as well as strong PAH emission bands. These apparently contradictory dust IR emission properties are discussed in terms of iron-poor silicate composition, carbon dust deficit, small grain size and low dust temperature in the young AGN phase of these three galaxies.

Subject headings: dust, extinction — galaxies: active — galaxies: individual (IRAS F10398+1455, IRAS F21013-0739, SDSS J0808+3948) — infrared: galaxies

1. Introduction

Active galactic nuclei (AGN) are postulated to have their central powering sources blocked by a dust torus. The dust reprocesses the ultraviolet (UV) and optical photons from the central engine and re-radiates in the infrared (IR). Different types of AGNs are proposed to be the same type of objects but viewed at different angles between the line of sight of an observer and the central engine (Antonucci 1993).

The 9.7 μm and 18 μm emission features detected in type 1 AGNs (Sturm et al. 2005, Siebenmorgen et al. 2005, Hao et al. 2005) are believed to originate from warm amorphous silicate dust.

[1]Shanghai Astronomical Observatory, Chinese Academy of Sciences, 80 Nandan Road, Shanghai 200030, China

[2]Department of Physics and Astronomy, University of Missouri, Columbia, MO 65211, USA

[†]haol@shao.ac.cn

In AGNs, some dust is hot enough to generate a strong, *flat* emission continuum in the 5–8 μm wavelength range, making it an effective diagnostic tool to distinguish AGN-dominated galaxies from starburst-dominated galaxies (e.g., see Laurent et al. 2000, Nardini et al. 2008). In addition to silicate dust, polycyclic aromatic hydrocarbon (PAH) molecules also display rich emission bands in the mid-IR (Tielens 2008, Wang et al. 2014). These features are usually very weak or absent in AGNs because PAHs are believed to have been destroyed by the harsh radiation field of AGNs. Compared to AGNs, starburst galaxies commonly display a low, *red* 5–8 μm emission continuum, strong PAH emission features and silicate *absorption* features (e.g. Brandl et al. 2006, Hao et al. 2007, Smith et al. 2007).

Here we report the simultaneous detection of a low, *red* ∼5–8 μm emission continuum and strong silicate *emission* features in three galaxies, IRAS F10398+1455, IRAS F21013-0739 and SDSS J0808+3948. They also exhibit strong PAH emission in the mid-IR. The IR spectral characteristics of these galaxies are unique or anomalous in the sense that they show silicate *emission* which is characteristic of AGNs while they also show a low, *red* ∼5–8 μm emission continuum and strong PAH emission which are characteristic of starburst galaxies. We summarize the observations and data reduction in §2. The analysis and results are presented in §3. We discuss the implications of these results in §4. The major conclusions are summarized in §5.

2. Observations and Data Reduction

The mid-IR spectra of the three sources were obtained with the *Infrared Spectrograph* (IRS) instrument on board the *Spitzer Space Telescope* (Houck et al. 2004). The IRS spectra cover the 5–40 μm wavelength range, with a spectral resolution that varies from ∼57 to ∼128. We use the data archived in the *Cornell AtlaS of Spitzer/IRS Sources* (CASSIS) where the spectra are extracted according to the extent of sources (Lebouteiller et al. 2011). The CASSIS atlas includes

Table 1. Basic Parameters for the Three Sources

Sources	RA	DEC	Redshift	AORKEY	$d_{\rm L}$[a] (Mpc)	$L_{\rm UV}$[b] (10^{43}ergs s^{-1})
IRAS F10398+1455	10h42m33.32s	+14d39m54.1s	0.099	22132992	456	2.05
IRAS F21013-0739	21h03m58.75s	-07d28m02.5s	0.136	23017216	640	16.5
SDSS J0808+3948	08h08m44.27s	39d48m52.36s	0.091	23014144	416	8.50

[a] Luminosity distance.

[b] GALEX Near-Ultraviolet (NUV) luminosity (taken from NED).

$\sim$13,000 low resolution spectra of >11,000 distinct sources observed in the standard staring mode and provides publishable quality spectra. Table 1 presents the basic parameters for the three sources.

3. Results

We show the IRS spectra of the three sources in Figure 1a. They all exhibit strong PAH emission features at 6.2 μm, 7.7 μm, 8.6 μm, 11.2 μm and 12.7 μm as well as the 9.65 μm $H_2S(3)$ rotational line. These are typical emission features of starburst galaxies. Several atomic emission features which are related to starburst activity are also detected in these three sources: [Ar II] 6.986 μm, [Ne II] 12.81 μm and [Ne III] 15.56 μm. The 10.51 μm [S IV] line is prominent in IRAS F10398+1455 and IRAS F21013-0739, but not seen in SDSS J0808+3948. No obvious high ionization-potential lines like [Ne V] 14.32 μm and [O IV] 25.89 μm (which are typical in AGNs) are detected in our three galaxies. Finally, the 9.7 μm and 18 μm amorphous silicate emission features are clearly seen in all three galaxies.

In Figure 1a we also compare the mid-IR spectra of these three galaxies with the averaged spectrum of starburst galaxies (Brandl et al. 2006) and the average spectrum of quasars (Hao et al. 2007). It is seen that our three sources have a comparable silicate emission strength as quasars, but they show a much steeper or "redder" 5–8 μm continuum than typical AGNs or quasars. The slope of the 5–8 μm continuum, defined as $d\ln F_\nu / d\ln\lambda$ (where F_ν is the observed flux and λ is wavelength), is $\sim$4.1–4.6 for the three sources, while the 5–8 μm continuum is flat or "gray" for AGNs (with a slope of $\sim$0.8). The "red" 5–8 μm emission continuum and the strong PAH emission features seen in these galaxies are also seen in starburst galaxies. However, the 9.7 μm and 18 μm emission features seen in these galaxies are never seen in starburst galaxies. Type 1 AGNs (and some type 2 AGNs; see Sturm et al. 2006, Mason et al. 2009, Nikutta et al. 2009, Shi et al. 2010) exhibit the silicate emission features seen in these galaxies, but their 5–8 μm emission continuum is often much flatter and do not show the PAH emission features which are prominent in these three galaxies.

The exact profiles and strengths of the derived silicate emission features are sensitive to the assumed underlying continuum (e.g., see Sirocky et al. 2008, Baum et al. 2010, Gallimore et al. 2010). To subtract the continuum, we take two approaches: (1) we select five points at 5–7 μm, 14.5–15.0 μm and 29–30 μm to define a underlying continuum which is calculated with a spline function (see Figure 2); (2) we modify the PAHFIT software of Smith et al. (2007) to fit the observed IRS spectrum of each source with a combination of PAH features, amorphous silicate features, modified blackbodies, and starlight, with the sum of the modified blackbodies and starlight representing the continuum underneath the PAH and silicate features (see Figure 3). Not surprisingly, the silicate emission features derived from these two approaches differ substantially: the 9.7 μm feature derived from the spline method is considerably weaker than that derived from the PAHFIT method, while it is in the opposite for the 18 μm feature. Nevertheless, it is clear that both the 9.7 μm and 18 μm

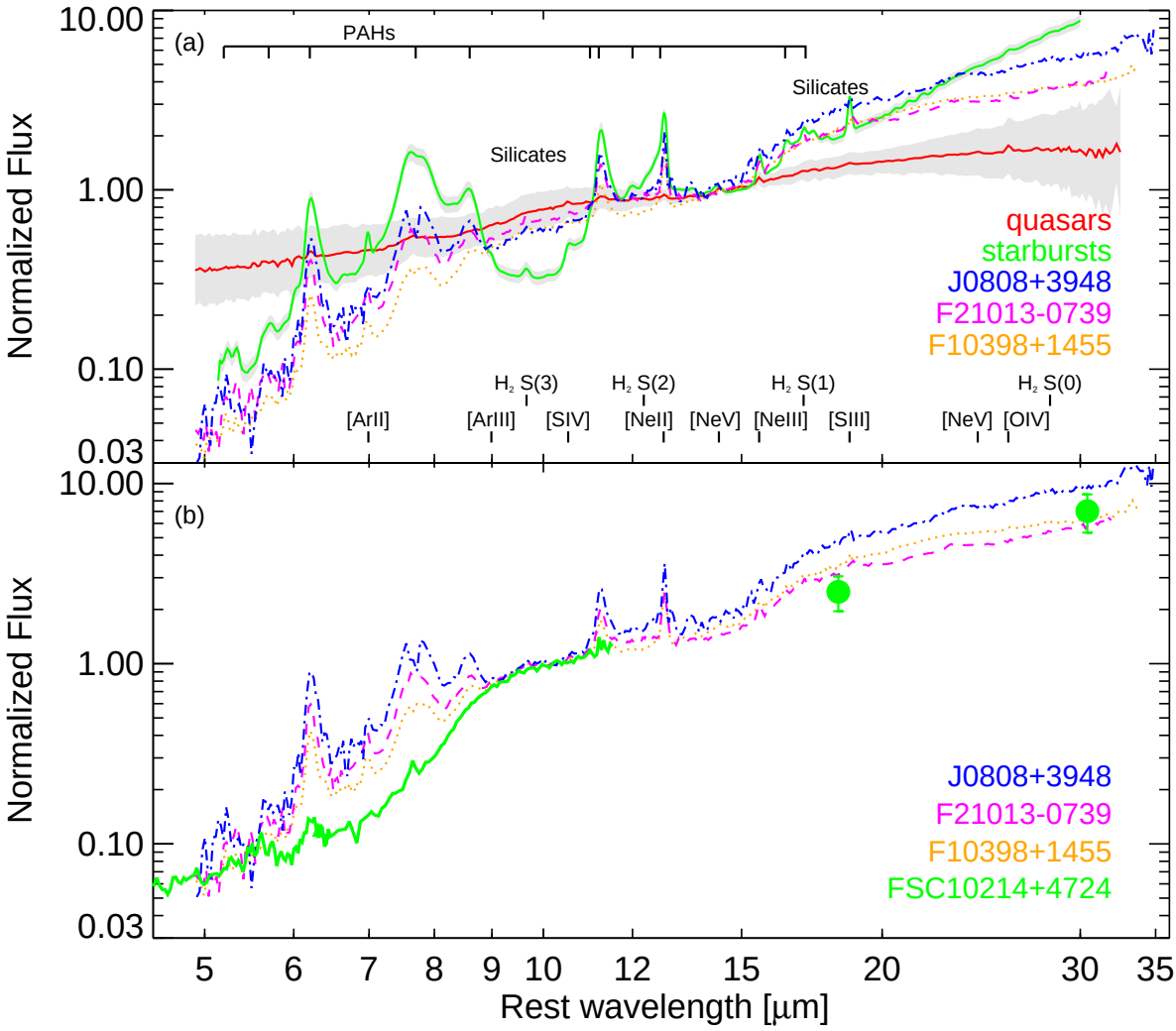

Fig. 1.— Upper panel (a): Comparison of the IRS spectra of SDSS J0808+3948 (blue), IRAS F21013-0739 (magenta), and IRAS F10398+1455 (orange), with the average spectrum of quasars (red; Hao et al. 2007) and the average spectrum of starburst galaxies (green; Brandl et al. 2006). All spectra are normalized at 14.5 μm. Bottom panel (b): Comparison of the IRS spectra of SDSS J0808+3948 (blue), IRAS F21013-0739 (magenta), and IRAS F10398+1455 (orange) with that of IRAS FSC 10214+4724 (green; Teplitz et al. 2006), a lensed ULIRG. Also shown are the IRAS 60 μm and 100 μm photometry of IRAS FSC 10214+4724 (filled green circles) with its redshift of $z \approx 2.29$ taken into account. All spectra are normalized at 10 μm.

amorphous silicate emission features are present in these three sources.

Crystalline forsterite silicates are also present in these galaxies as revealed by the sharp features at ∼19, 23, and 27.5 μm (see Figures 2, 3). The detection of crystalline silicate dust in extragalactic sources has been reported for some ULIRGs (Spoon et al. 2006), for PG 2112+059, a broad absorption line quasar (Kemper et al. 2007), for a distant absorber at redshift $z_{\rm abs} \approx 0.886$ along the line of sight toward the gravitationally lensed quasar PKS 1830-211 (Aller et al. 2012), and for a $z_{\rm abs} \approx 0.685$ absorber toward the gravitationally lensed blazar TXS 0218+357 (Aller et al. 2014).

In the Galactic ISM the silicate dust is predominantly amorphous (Li & Draine 2001, Kemper et al. 2004, Li et al. 2007). As shown in Figures 2, 3, the silicate features of these three galaxies are broad and smooth with sharp crystalline silicate features superimposed, suggesting that the silicate dust in these sources is mainly amorphous.

4. Discussion

These three galaxies are found when cross-matching the SDSS and *Spitzer*/IRS low resolution spectra (L. Hao et al. 2014, in preparation). Xie et al. (2014a) have studied the multi-wavelength properties of these three galaxies and demonstrated that they may harbor a young AGN at the center. Among these galaxies, IRAS F21013-0739 and SDSS J0808+3948 are *Lyman Break Analogs* (LBA; Heckman et al. 2005, Hoopes et al. 2007). LBAs are rare in the local universe. They are selected based on their far-UV properties and they show similar properties as that of high-redshift *Lyman Break Galaxies* (Steidel et al. 1999). Among the 30 LBA galaxies, six are found to contain a young, very compact ($\sim 10^2$ pc), highly massive (several 10^9 $M_\odot$) *Dominant Central Object* (DCO, Overzier et al. 2009). Interestingly, both F21013-0739 and SDSS J0808+3948 are found to have DCOs. It appears that the occurrence of the anomalous mid-IR spectral character is associated with the galaxies with a DCO. IRAS F10398+1455 is not a LBA. This galaxy is very faint in the GALEX Far-UV (FUV) band but it is bright in the GALEX NUV band. We list the NUV luminosity in Table 1 for the three galaxies. It is unresolved in the NUV image and its light distribution is comparable to that of IRAS F21013-0739 and that of the GALEX standard star, indicating a compact UV region in this galaxy.

The type of spectrum (i.e., a combination of a *red* 5–8 μm continuum with strong silicate *emission*) found for the three galaxies reported here is very rare. To the best of our knowledge, the only similar source is IRAS FSC 10214+4724, a lensed ULIRG at a redshift of $z \approx 2.29$ (Teplitz et al. 2006), which shows a red 5–8 μm emission continuum and strong silicate emission features. However, little or no PAH emission is seen in this source (see Figure 1b). Teplitz et al. (2006) showed that the silicate emission features of this source are similar to that of other AGNs observed by *Spitzer*/IRS. They fitted the near-IR to $\lambda \approx 365\,\mu$m rest-frame spectral energy distribution (SED) of this source with a combination of hot dust ($T \approx 640$ K), warm dust ($T \approx 190$ K) and cold

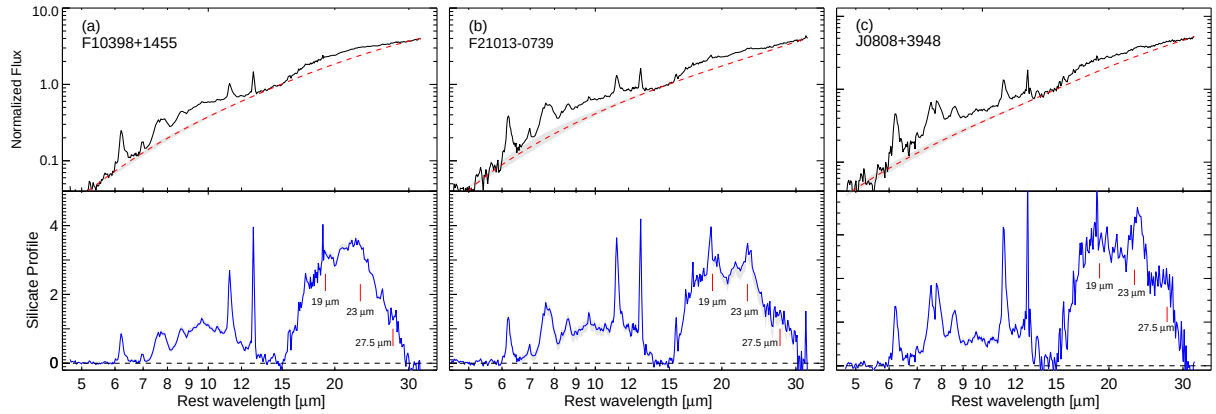

Fig. 2.— The IRS spectra and the underlying *spline* continuum (upper panel) as well as the continuum-subtracted silicate emission profiles (bottom panel) of IRAS F10398+1455 (a), IRAS F21013-0739 (b) and SDSS J0808+3948 (c). The PAH features at 6.2, 7.7, 8.6, 11.3 and 12.7 μm and the crystalline silicate features at 19, 23 and 27.5 μm are prominent.

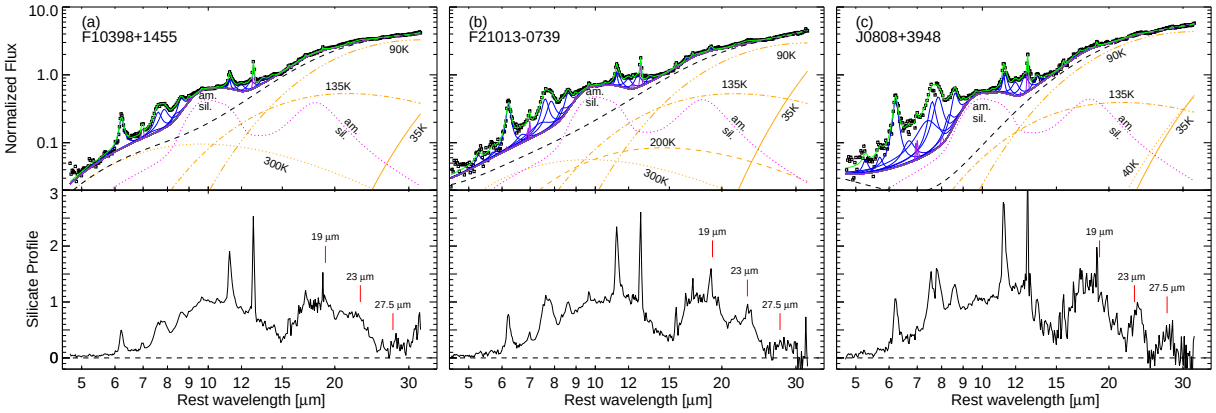

Fig. 3.— Same as Figure 2 but with the underlying continuum determined by fitting the IRS spectra with a combination of PAH features (solid blue lines), amorphous silicate features (dotted magenta lines), modified blackbodies of different temperatures, and starlight (upper panel). The sum of the modified blackbodies and starlight represents the continuum underneath the PAH and silicate features (dashed black line). The continuum-subtracted silicate emission profiles are shown in the bottom panel.

dust ($T \approx 50\,\mathrm{K}$). They found that the contribution of the hot dust component to the SED which is directly related to AGN heating and accounts for the 2–8 μm continuum emission is rather small compared to other AGN-dominated ULIRGs and QSOs. If most of the IR luminosity of IRAS FSC 10214+4724 is due to starburst, it is difficult to understand why the PAH emission which is strong in starbust galaxies is rather weak in FSC 10214+4724.

Teplitz et al. (2006) explained the unusual spectral characteristics of IRAS FSC 10214+4724 (i.e., a *red* 2–8 μm continuum, strong silicate *emission*, little or no PAH emission) in terms of differential lens magnification that magnifies the central AGN features (e.g., the silicate emission), while masking the starburst signatures with unusually weak PAH emission. But this hypothesis could not explain the weak, red 2–8 μm continuum (i.e., the hot dust component) which is believed to be closely tied with the central AGN.

The differential lens magnification scenario may not work for our three sources since all three galaxies are at low redshifts, from $z \approx 0.091$ to $z \approx 0.137$, and there are no galaxy clusters lying along the line of sight toward these three galaxies (see Yang et al. 2007).

The combination of a steeply rising red 5–8 μm emission continuum with the silicate emission features at 9.7 and 18 μm suggests the dust temperature is in the range of $\sim$100–300 K. In contrast, the flat 5–8 μm emission and the silicate emission of quasars shown in Figure 1a imply a dust temperature of $\sim$300–500 K. For illustration, we show in Figure 3a the thermal IR emission of spherical "astronomical silicates" (Draine & Lee 1984) of radius $a = 0.1\,\mu$m at temperatures $T = 100$, 250, and 500 K. The dust IR emission is expressed as $\kappa_{\rm abs}(\nu) \times B_\nu(T)$ and normalized to that at $\lambda = 9.8\,\mu$m, where $\kappa_{\rm abs}(\nu)$ is the mass absorption coefficient of the dust at frequency $\nu = c/\lambda$ (c is the speed of light), and $B_\nu(T)$ is the Planck function of temperature T at frequency ν. Figure 3a shows that with the increase of T, the 2–8 μm continuum emission becomes stronger and flatter.

The temperature of the dust in an AGN torus ranges from the sublimation temperature of $T \approx 1500\,\mathrm{K}$ in the inner wall to $T \approx 100\,\mathrm{K}$ in the outer boundary (Li 2007). Depending on how the dust is spatially distributed in the torus, the appearances of the 5–8 μm continuum and the silicate emission features would differ from one to another. For the three galaxies reported here, a simple explanation would be that the dust tori of the AGNs in these galaxies are at a larger distance from the central engine compared to that of typical AGNs and quasars.

Alternatively, the difference between the average IRS spectrum of quasars and the IRS spectra of our three galaxies could be due to different silicate composition. Dorschner et al. (1995) have experimentally demonstrated that the absorption in the UV, optical and near-IR up to $\lambda < 8\,\mu$m of amorphous silicate dust decreases with the decrease of the iron content in the dust. As shown in Figure 4 of Dorschner et al. (1995), the imaginary part of the index of refraction of $MgSiO_3$ is smaller than that of $Mg_{0.4}Fe_{0.6}SiO_3$ by a factor of > 10. It is possible that the silicate dust in quasars and typical AGNs are iron-rich, while the silicate dust in the three galaxies are iron-poor. In Figure 3b we show the mass absorption coefficients calculated for three amorphous pyroxene

dust species: $MgSiO_3$, $Mg_{0.7}Fe_{0.3}SiO_3$, and $Mg_{0.4}Fe_{0.6}SiO_3$, with the refractive indices taken from Dorschner et al. (1995). All dust species are assumed to be spherical and have a radius of $a = 0.1\,\mu$m. It is apparent that the continuum absorption at $\lambda < 8\,\mu$m substantially increases with the iron content. We note that the Draine & Lee (1984) "astronomical silicates" were synthesized to be "dirty" so that they are absorptive in the UV, optical and near-IR.

The 5–8 μm emission continuum difference between these three galaxies and typical AGNs and quasars may also be accounted for by different fractions of amorphous carbon or graphite dust. In addition to amorphous silicate dust, there must be a population of carbonaceous dust in the Galactic ISM (see Li 2005). Although the exact nature of the carbonaceous dust species is unknown, graphite and amorphous carbon are commonly suggested as candidates. In the 0.1–8 μm wavelength range, as shown in Figure 3c, both amorphous carbon and graphite have a much higher absorption opacity than amorphous silicate dust (including Fe_2SiO_4 and $FeSiO_3$). We take the indices of refraction of amorphous carbon and graphite respectively from Rouleau & Martin (1991) and Draine & Lee (1984). The low 5–8 μm continuum emission observed in these three galaxies could be attributed to a relative deficit of carbon dust compared to that of typical AGNs/quasars.

The IRS spectral appearance difference between these three galaxies and typical AGNs/quasars could also be due to dust size effects. Dust absorbs and scatters light most effectively at wavelengths comparable to its size ($2\pi a/\lambda \sim 1$; see Bohren & Huffman 1983). As illustrated in Figure 3d, the absorption of large "astronomical silicate" dust of $a \gtrsim 1\,\mu$m in the 2–8 μm wavelength range substantially exceeds that of submicron-sized dust. For silicate dust of $a \gtrsim 5\,\mu$m, the absorption at $\lambda < 8\,\mu$m is "gray" and the 9.7 μm silicate feature is very broad and weak. The strong, flat 5–8 μm emission continuum seen in quasars could be dominated by dust of sizes $a \gtrsim 1\,\mu$m, while the low, red 5–8 μm continuum seen in these three galaxies may indicate that they are rich in submicron-sized dust.

We note that the above analysis on the dust composition is somewhat simplified. It is known that radiative transfer effects could account for some of the "anomalous" spectral characteristics of AGNs, e.g., Nikutta et al. (2009) demonstrated that the apparent red-shift of the 9.7 μm silicate emission feature of AGNs (Hao et al. 2005, Siebenmorgen et al. 2005, Sturm et al. 2005) could be due to radiative transfer effects, although it could also be due to porous dust (see Li et al. 2008) or micrometer-sized dust (see Smith et al. 2010). To more reliably determine the dust composition from the observed IRS spectrum of a source, one needs to combine the dust optical properties with proper radiative transfer. However, we have demonstrated in Y. Xie et al. (2014, in preparation) that it is not possible to simultaneously fit both the silicate emission features and the red 5–8 μm continuum with the radiative transfer models of Nenkova et al. (2008a, b) for clumpy tori and with the silicate optical properties of Ossenkopf et al. (1992). Models that fit the silicate emission well will always overestimate the 5–8 μm continuum observed in the three sources. Therefore, we believe that the anomalous spectral characteristics (i.e., a red 5–8 μm continuum, strong silicate emission, strong PAH emission) of these three sources are potentially revealing anomalous dust properties intrinsic to them.

Finally, we note that both PAH and silicate emission features are strong in the three galaxies (see Figure 2), in contrast to the absence of PAH emission in normal AGNs. It is generally believed that PAHs are destroyed by the AGN hard radiation field. The survival of PAHs in these three galaxies may be due to the fact that they are at the young AGN/starburst phase of their evolution. Or alternatively, the region covered by the *Spitzer*/IRS slit may contain parts of the starburst region which emits strongly in PAH features.

5. Summary

We report *Spitzer*/IRS detections of anomalous dust properties in three galaxies (IRAS F10398+1455, IRAS F21013-0739, and SDSS J0808+3948) which harbor young AGN and starburst activity. Unlike most other starburts or AGNs observed thus far with *Spitzer*/IRS, these three galaxies exhibit a red 5–8 μm emission continuum and strong silicate and PAH emission. The red 5–8 μm emission continuum and PAH emission seen in these galaxies are characteristic of starbursts. However, for starbursts the silicate features are often seen in absorption. The silicate emission seen in these galaxies is characteristic of AGNs, but for AGNs the 5–8 μm emission continuum is often flat (or "gray") and the PAH emission features are often absent. We argue that these apparently contradictory properties of these three galaxies may be explained by iron-poor silicate dust, a relative deficit of amorphous carbon or graphite dust, and/or cold, submicron-sized dust.

We thank J.W. Lyu, R. Mason, A. Mishra and the anonymous referee for helpful suggestions/discussions. LH and XYX are partially supported by the 973 Program of China (2013CB834905, 2009CB824800), the Strategic Priority Research Program "The Emergence of Cosmological Structures" of Chinese Academy of Sciences (XDB09000000), the Shanghai Pujiang Talents Program (10pj1411800) and NSFC 11073040. AL and XYX are supported in part by NSF AST-1311804 and NASA NNX14AF68G. The Cornell Atlas of *Spitzer*/IRS Sources (CASSIS) is a product of the Infrared Science Center at Cornell University, supported by NASA and JPL.

REFERENCES

Antonucci, R. 1993, ARA&A, 31, 473

Aller, M. C., et al. 2012, ApJ, 748, 19

Aller, M. C., et al. 2014, ApJ, 785, 36

Baum, S. A., et al. 2010, ApJ, 710, 289

Brandl, B. R., et al. 2006, ApJ, 653, 1129

Bohren, C. F. & Huffman, D. R. 1983, Absorption and scattering of light by small particles, Wiley

Draine, B. T. & Lee, H. M. 1984, ApJ, 285, 89

Dorschner, J., et al. 1995, A&A, 300, 503

Gallimore, J. F., et al. 2010, ApJS, 187, 172

Hao, L., et al. 2005, ApJ, 625, L75

Hao, L., et al. 2007, ApJ, 655, L77

Heckman, T. M., et al. 2005, ApJ, 619, L35

Hoopes, C., et al. 2007, ApJS, 173, 441

Houck, J. R., et al. 2004, ApJS, 154, 18

Kemper, F., Vriend, W. J. & Tielens, A. G. G. M. 2004, ApJ, 609, 826

Laurent, O., et al. 2000, A&A, 359, 887

Lebouteiller, V., et al. 2011, ApJS, 196, 8

Li, A. 2005, Journal of Physics Conference Series, 6, 229

Li, A. 2007, in The Central Engine of Active Galactic Nuclei (ASP Conf. Ser. 373), ed. L. C. Ho & J.-M. Wang (San Francisco, CA: ASP), 561

Li, A. & Draine, B. T. 2001, ApJ, 550, L213

Li, M. P., Zhao, G. & Li, A. 2007, MNRAS, 382, L26

Li, M. P., Shi, Q. J. & Li, A. 2008, MNRAS, 391, L49

Molster, F. & Kemper, C. 2005, Space Sci. Rev., 119, 3

Markwick-Kemper, F., et al. 2007, ApJ, 668, L107

Mason, R. E., et al. 2009, ApJ, 693, L136

Nardini, E., et al. 2008, MNRAS, 385, L130

Nenkova, M., Sirocky, M. M., Ivezić, Ž., & Elitzur, M. 2008a, ApJ, 685, 147

Nenkova, M., Sirocky, M. M., Nikutta, R., Ivezić, Ž., & Elitzur, M. 2008b, ApJ, 685, 160

Nikutta, R., et al. 2009, ApJ, 707, 1550

Ossenkopf, V., Henning, T., & Mathis, J. S. 1992, A&A, 261, 567

Overzier, R. A., et al. 2009, ApJ, 706, 203

Rouleau, F. & Martin, P. G. 1991, ApJ, 377 526

Shi, Y., et al. 2010, ApJ, 714, 115

Sirocky, M. M, et al. 2008, ApJ, 678, 729

Smith, H. A., et al. 2010, ApJ, 716, 490

Smith, J. D. T., et al. 2007, ApJ, 656, 770

Spoon, H. W. W., et al. 2006, ApJ, 638, 759

Steidel, C. C., et al. 1999, ApJ, 519, 1

Sturm, E., et al. 2005, ApJ, 629, L21

Sturm, E., et al. 2006, ApJ, 642, 81

Siebenmorgen, R., et al. 2005, A&A, 436, L5

Teplitz, H. I., et al. 2006, ApJ, 638, L1

Tielens, A. G. G. M. 2008, ARA&A, 46, 289

Wang, M.L., Li, A., Xiang, F.Y., Tang, Y., & Zhong, J.X. 2014, Scientia Sinica – Physica, Mechanica & Astronomica, 44, 771

Yang, X., et al. 2007, ApJ, 671, 153

This preprint was prepared with the AAS LaTeX macros v5.2.

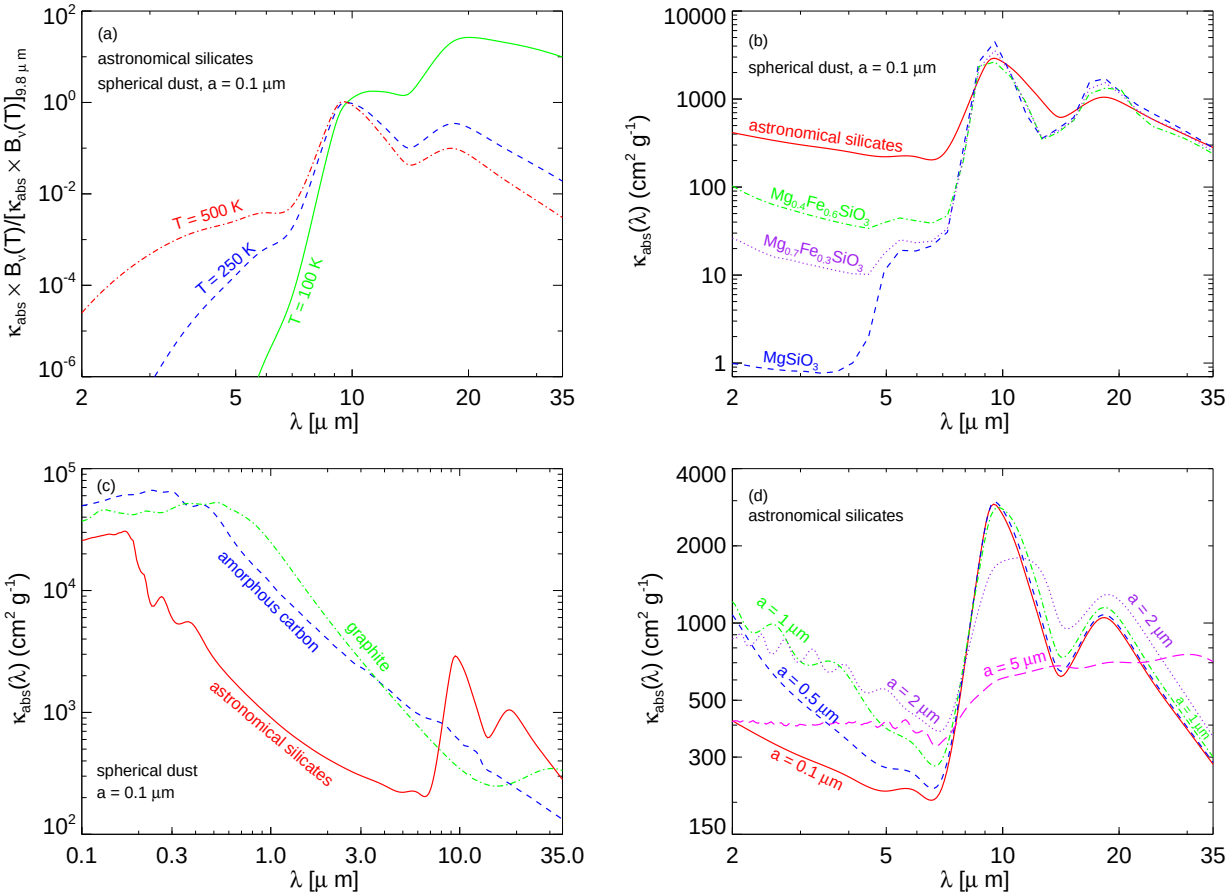

Fig. 4.— Upper left panel (a): Normalized IR emission spectra of spherical "astronomical silicates" of radius $a = 0.1\,\mu$m of temperatures $T = 100\,$K (green solid), 250 K (blue dashed), and 500 K (red dot-dashed). Upper right panel (b): Mass absorption coefficients of "astronomical silicates" (red solid) and amorphous pyroxenes of varying iron contents: $MgSiO_3$ (blue dashed) , $Mg_{0.7}Fe_{0.3}SiO_3$ (purple dotted), and $Mg_{0.4}Fe_{0.6}SiO_3$ (green dot-dashed). All dust species are taken to be spherical with $a = 0.1\,\mu$m. Bottom left panel (c): Mass absorption coefficients of "astronomical silicates" (red solid), amorphous carbon (blue dashed), and graphite (green dot-dashed). All dust species are taken to be spherical with $a = 0.1\,\mu$m. Bottom right panel (d): Mass absorption coefficients of spherical "astronomical silicates" of various sizes: $a = 0.1\,\mu$m (red solid), $a = 0.5\,\mu$m (blue dashed), $a = 1\,\mu$m (green dot-dashed), $a = 2\,\mu$m (purple dotted), and $a = 5\,\mu$m (magenta long dashed).